Electronic Supplementary Information

Sluggish anion transport provides good kinetic stability to the anhydrous anti-perovskite solid electrolyte Li_3OCl

J. A. S. Serejo, J. S. Pereira, R. Mouta and L. G. C. Rego

SUMMARY

1 Force-field calculations

The Gibbs energy per formula unit (f.u.) for the crystal without defects, G_0, consists of the static and vibrational contributions. They are, respectively, the lattice internal energy/f.u., U_{lat}, and the phonon Helmholtz energy/f.u., F_{vib}:

$$G_0 = U_{lat} + pV + F_{vib}, \quad (1)$$

where p is the external pressure (1 bar in this work) and V is the volume/f.u.

In this work, U_{lat} is approximated to the lattice potential energy/f.u that has contributions from individual ions and pairwise interactions. The former arises from the atomic polarization of O^{2-} and Cl^-, as described by the shell model (the less polarizable Li^+ was modelled as a rigid ion). Within such model,[1] each ion is comprised of a core (nucleus and innermost electrons) and a shell (remaining electrons) that may be displaced from one another by a distance d, in which case a harmonic potential energy U_i^H with force constant k is assumed:

$$U_i^H = k_i d_i^2/2\,. \quad (2)$$

The pairwise interactions consist of a superposition of electrostatic (U_{ij}^E) and Buckingham (U_{ij}^B) potentials,

$$U_{ij}^B = A_{ij}\,exp\left(-r_{ij}/\rho_{ij}\right) - C_{ij}/r_{ij}^6\,, \quad (3)$$

where r is the distance between the pair of ions and A, ρ and C are fitting parameters that depend only on the interacting species. The first term is the Born-Mayer potential (U_{ij}^{BM}). It is short-ranged and was summed only over neighbours within a cut-off radius

of 12 Å. The second term is the Van der Waals potential (U_{ij}^{V}) that acts only on the polarizable ions O^{2-} and Cl^{-}. U_{ij}^{V} and U_{ij}^{E} are summed according to the Ewald method. Therefore, for Li_3OCl, U_{lat} is given by

$$U_{lat} = U_{O}^{H} + U_{Cl}^{H} + \frac{1}{2}\sum_{j}\left(3U_{Li,j}^{E} + U_{O,j}^{E} + U_{Cl,j}^{E}\right) + \frac{1}{2}\sum_{\substack{j \\ r\leq 12\,\text{Å}}}\left(3U_{Li,j}^{BM} + U_{O,j}^{BM} + U_{Cl,j}^{BM}\right) + \frac{1}{2}\sum_{j}\left(U_{O,j}^{V} + U_{Cl,j}^{V}\right). \quad (4)$$

Here, the subscripts "Cl" and "O" designate the Cl^{-} and O^{2-} ions inside the unit cell and "Li" represents one of the three symmetry-equivalent Li^{+} ions inside the unit cell. The sums are over pairwise interactions, thereby divided by 2 to correct for double counting. The electrostatic and Van der Waals sums extend to infinity in the Ewald framework.

F_{vib} , in eqn. (1), is calculated within the quasi-harmonic approximation, in which the cell parameters are adjusted to minimize the vibrational Gibbs energy, G_{vib}, while the lattice vibrations are assumed to be harmonic. Thus, F_{vib} can be derived from the harmonic vibrational partition function, Z_{vib}. The starting point is the partition function for a single quantum harmonic oscillator of phonon mode m and wavevector $\boldsymbol{k}$,[2]

$$z_{\boldsymbol{k}m} = \frac{\exp\left(-\frac{\beta h\nu_{\boldsymbol{k}m}}{2}\right)}{1-\exp(-\beta h\nu_{\boldsymbol{k}m})}, \quad (5)$$

where $\beta = (k_B T)^{-1}$. Each unit cell of the crystal contributes with 3n vibrational modes, where n is the number of ions in the unit cell. Thus, we define $z_{\boldsymbol{k}} = \prod_m z_{\boldsymbol{k}m}$ as the vibrational partition function of the unit cell, which has to be averaged over all the wavevectors of the Brillouin zone to yield the total vibrational partition function

$$Z_{vib} = \prod_{\boldsymbol{k}}(z_{\boldsymbol{k}})^{w_{\boldsymbol{k}}}, \quad (6)$$

where the sum over the weights $w_{\boldsymbol{k}}$ is equal to 1. This leads to:

$$F_{vib} = -\frac{1}{\beta}\ln(Z_{vib}) = \sum_{\boldsymbol{k},m} w_{\boldsymbol{k}}\left\{\frac{h\nu_{\boldsymbol{k}m}}{2} + \frac{1}{\beta}\ln[1-\exp(-\beta h\nu_{\boldsymbol{k}m})]\right\}. \quad (7)$$

F_{vib} can also be expressed in terms of the vibrational internal energy/f.u. (U_{vib}), the entropy/f.u. (S_{vib}), and the temperature (T) as $F_{vib} = U_{vib} - TS_{vib}$, with U_{vib} and S_{vib} given by:

$$U_{vib} = \sum_{\boldsymbol{k},m} w_{\boldsymbol{k}}\left[\frac{h\nu_{\boldsymbol{k}m}}{2} + \frac{h\nu_{\boldsymbol{k}m}}{\exp(\beta h\nu_{\boldsymbol{k}m})-1}\right]; \quad (8)$$

$$S_{vib} = k_B\sum_{\boldsymbol{k},m} w_{\boldsymbol{k}}\left\{\frac{\beta h\nu_{\boldsymbol{k}m}}{\exp(\beta h\nu_{\boldsymbol{k}m})-1} - \ln[1-\exp(-\beta h\nu_{\boldsymbol{k}m})]\right\}. \quad (9)$$

A 4×4×4 Monkhorst–Pack[3] **k**-point grid was used to calculate the vibrational properties. Defining the total Helmholtz energy/f.u. as $F_0 = U_{lat} + U_{vib} - TS_{vib}$, G_0 can be expressed as:

$$G_0 = F_0 + pV. \quad (10)$$

In equilibrium, the internal pressure

$$p_{int} = -\partial F_0/\partial V \quad (11)$$

must balance the external pressure p.

The algorithm for G_0 minimization goes as follows. First, the equilibrium F_0 relative to the internal coordinates (those of cores and shells) is calculated for different sets of cell parameters to obtain p_{int}. Every F_0 evaluation requires a phonon calculation. Next, V is varied isotropically until $p_{int} = p$. Then, G_0 is minimized with respect to the unit cell parameters while internal coordinates are kept at minimum internal energy positions (ZSISA approximation).[2,4–6]

We used the Mott-Littleton method to calculate defect Gibbs energies. It consists of dividing the crystal into regions. The defect lies in the inner spherical region (region 1), where all interactions are calculated explicitly, and relaxations are constrained only by the crystal symmetry. It is surrounded by a thick spherical shell (region 2a) where all interactions are also calculated explicitly, but relaxations follow harmonic displacements. In the remainder of the crystal (region 2b), only the polarization of sublattices as due

to the charged defect is taken into account in the defect Gibbs energy. Here, the inner and outer limits of region 2a were 16.5 Å e 18.5 Å. For each calculation, we centred region 1 at the average of all defect positions. Contrary to supercell calculations, where the perfect cell energy must be subtracted from the defect-containing one to obtain the defect energy, the output energies here were already the defect energies.

Gibbs energies of migration were calculated by subtracting the defect's Gibbs energy of formation from the Gibbs energy at saddle point along the migration path. Each point of the Gibbs energy barrier profiles was obtained by constraining one of the migrating ion coordinates and letting all remaining coordinates in the Mott-Littleton regions 1 and 2a to relax.

All Buckingham potential and atomic model parameters used here were derived by Mouta et *al*. [7] and are reproduced in **Table S1** and **Table S2**, respectively.

Table S1. Buckingham potential parameters.

Interaction	A (eV)	ρ (Å)	C (eVÅ^6)	Ref.
$O^{2-} - O^{2-}$	22764.3000	0.14900	13.185	7
$Cl^- - Cl^-$	5145.2755	0.30660	20.523	7
$Li^+ - O^{2-}$	433.2627	0.31384	0.000	7
$Li^+ - Cl^-$	421.0366	0.33640	0.000	7
$Li^+ - Li^+$	360.5269	0.16098	0.000	7

Table S2. Parameters for the shell and rigid ion models.

Ion	k (eV/ Å^2)	Y (eV)	X (eV)	Ref.
Li^+	-	-	1.000	7
O^{2-}	593.716	-2.183	0.183	7
Cl^-	39.444	-2.535	1.535	7

2 Further details on long- and short-range anion transport

2.1 On the discontinuity in the migration barrier via Path L3

The discontinuity around the fractional coordinate x = 0.11 of the migrating O^{2-} ion, evinced in Fig. S1, is due to a sudden change in the local environment around the O^{2-} ion. At x = 0.10, two Cl^- and one of the Li^+ ions are closer to the O^{2-} ion, resulting in higher interaction energy. On the other hand, at x = 0.12 these three ions move away, thereby decreasing their interaction energy with the migrating O^{2-}.

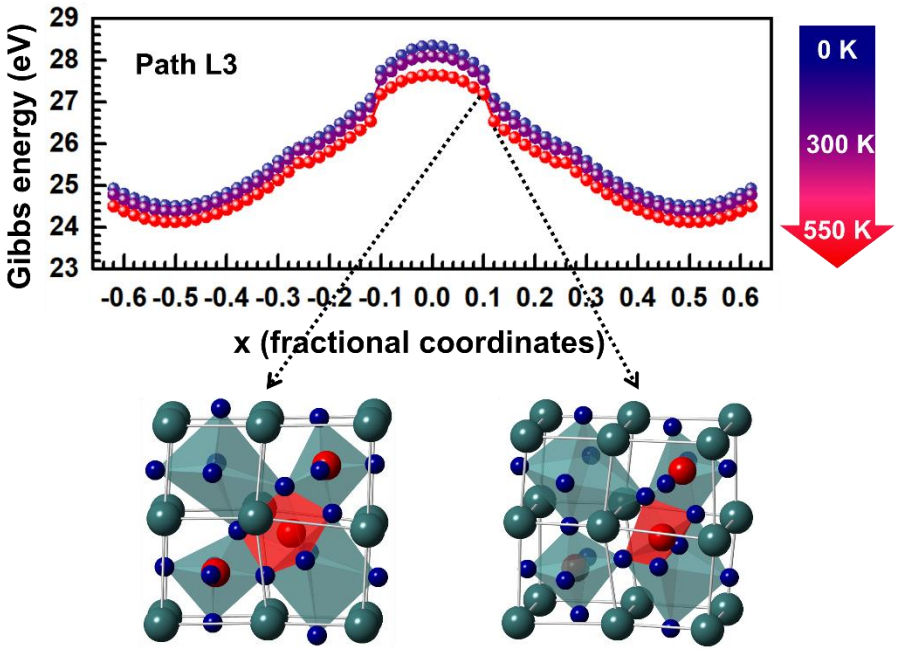

Fig. S1. Barrier profile discontinuity for the O^{2-} ion migration through path L3. The insets shown the local configurations for x = 0.10 (left) and x = 0.12 (right).

2.2 Vacancy-assisted reduction of the Gibbs energy of Cl^- migration (via Path L1a)

Since Li^+ vacancies co-exist with Cl^- vacancies, we also studied the latter's migration in the vicinity of the former. The Gibbs energy of migration *via* this path, termed Path L1a in Fig. 1 of the main text, is slightly reduced as compared to Path L1. The Gibbs energy barrier profile and selected relaxed configurations are shown in Fig. S2.

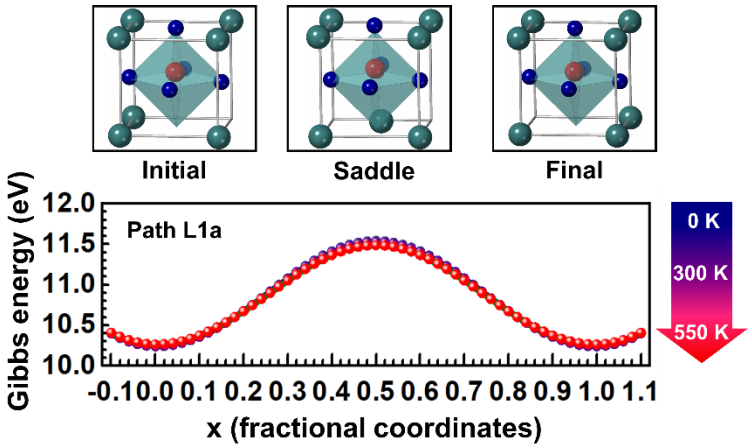

Fig. S2. Path L1a and its Gibbs energy barrier profile. This path is identical to L1, except for the presence of a Li^+ vacancy.

2.3 A fourth long-range transport mechanism

In principle, there is also a fourth known mechanism for cation migration in perovskites that could have an anion analogue in anti-perovskites, in which A- and B-site ion vacancies diffuse together, as Kilo *et al.* have shown with molecular dynamics simulations for Sr- and Mg-doped $LaGaO_3$ (i.e., $La_{1-x}Sr_xGa_{1-y}Mg_yO_{3-z}$, usually termed LSGM).[8] However, the analogue mechanism in Li_3OCl would require the existence of both Cl^- and O^{2-} vacancies in significant concentrations, and no energetically favourable defect can form them simultaneously in Li_3OCl. Therefore, we did not explore this migration mechanism here.

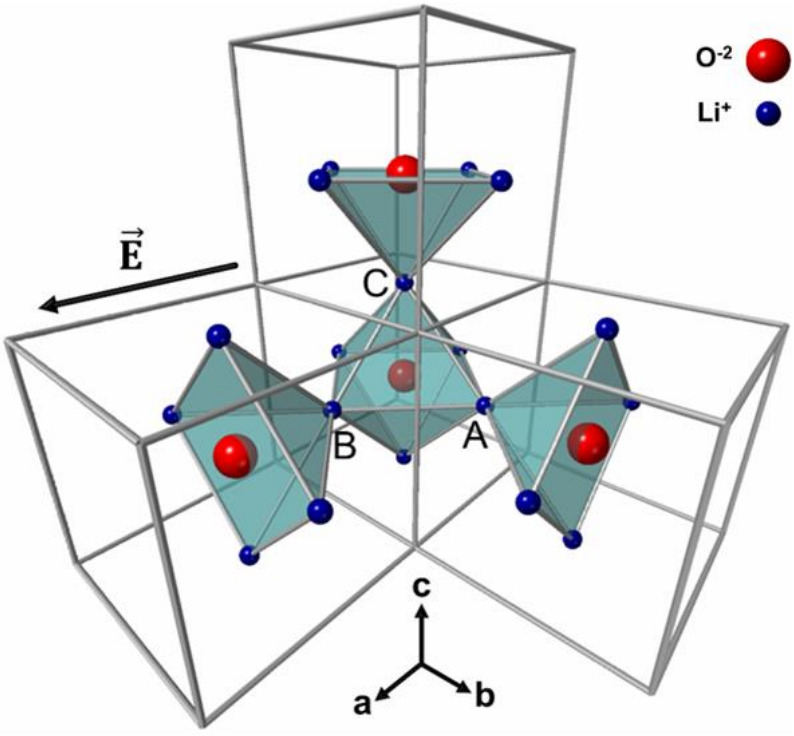

Fig. S3. Crystal structure of the Li_3OCl, depicting the three possible Li^+ ion positions in the cubic unit cell (A, B and C) and all their nearest-neighbour Li^+ ion positions. Mobilities are calculated for one Li^+ vacancy in either of the three positions. Cl^- ions were omitted for the sake of clarity.

3 On the calculation of vacancy mobilities in Li_3OCl

3.1 Mean electrical mobility of Li^+ vacancies

The electrical mobility of a Li^+ vacancy, μ_{Li}, depends on how efficiently it can move in the direction of the external electric field. As such, it is position-dependent. One can, however, calculate its mean value, $\langle\mu_{Li}\rangle$, by averaging over all possible Li^+ vacancy positions inside the unit cell, as done next. Another option would be to derive the atomistic expression for diffusivity and then using the Einstein relation to obtain the mean mobility. For instance, for the case discussed in this section, where the crystal structure has cubic symmetry and all vacancy positions correspond to the same Wyckoff site, this second approach would reduce the calculation effort by two-thirds. However, we chose the first approach as a groundwork for future studies where the symmetry is not cubic, or vacancies distribute themselves among different Wyckoff sites.

Let us consider the crystal structure of Li_3OCl, as shown in Fig. S3. The unit cell of Li_3OCl contains three Li^+ ions, which is the number of Li^+ ions per formula unit of the compound. Although there are six Li^+ ions, one on each face of the cubic cell, only three belong to a given unit cell whereas the other three belong to the neighbouring cells. Therefore, to obtain $\langle\mu_{Li}\rangle$, we must first calculate the mobility of the Li^+ ion vacancies associated with each of the three representative positions in the central unit cell in Fig. S3, namely A, B, and C.

We start by considering the mobility of a Li^+ ion vacancy at position A. Such vacancy can move to any of the eight nearby Li^+ ion positions, labelled from B to E and from G to H in Fig. S4. By symmetry, the energy of migration from A to any one of them is the same. Therefore, the defect mobility is given by [9,10]

$$\mu_A = \frac{|e|\nu\beta}{2}\sum_{\gamma}\left|\rho_{A\to\gamma}\right|^2 exp\left(-\beta G^m_{A\to\gamma}\right) = \frac{|e|\nu\beta}{2}exp(-\beta G^m_{Li})\sum_{\gamma}\left|\rho_{A\to\gamma}\right|^2. \tag{12}$$

In the equation above, $|e|$ is the proton charge (charge of a Li^+ ion vacancy), ν is the attempt frequency, G^m_{Li} is the Gibbs energy of migration of a Li^+ vacancy, $\beta = k_B T$, and

$$\left|\rho_{A\to\gamma}\right| = \left|(\vec{r}_\gamma - \vec{r}_A)\cdot\hat{E}\right| \tag{13}$$

is the displacement distance along the electric field direction $\hat{E}$, which is assumed to be along the crystal axis $\vec{a}$ – without loss of generality – and $(\vec{r}_\gamma - \vec{r}_A)$ is the displacement vector of migration from A to a neighbouring site γ.

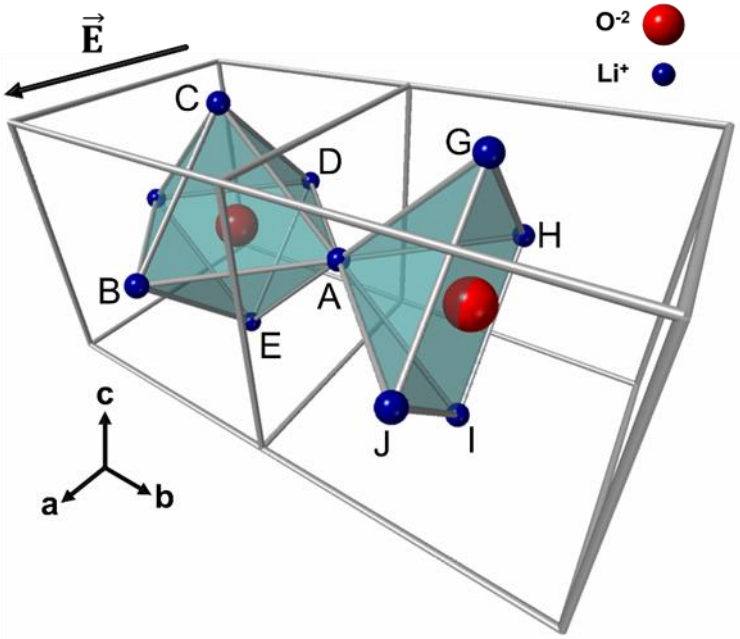

Fig. S4. Scheme utilized to calculate the mobility of a Li+ ion vacancy (not shown) at position A, based on the eight neighbouring positions to which such vacancy can hop, namely B, C, D, E, G, H, I, and J.

The displacement vector of migration from A to either C, E, G or I is perpendicular to the electric field, therefore

$$|\rho_{A\to C}|^2 = |\rho_{A\to E}|^2 = |\rho_{A\to G}|^2 = |\rho_{A\to I}|^2 = 0. \tag{14}$$

The vacancy displacement distance along $\hat{E}$ from A to either B, D, H or J is half a lattice parameter, leading to

$$|\rho_{A\to B}|^2 = |\rho_{A\to D}|^2 = |\rho_{A\to H}|^2 = \left|\rho_{A\to J}\right|^2 = \frac{a^2}{4}. \tag{15}$$

Summing over all eight positions, we get

$$\sum_{j=Y} |\rho_{A\to Y}|^2 = \frac{a^2}{4} + \frac{a^2}{4} + \frac{a^2}{4} + \frac{a^2}{4} = a^2. \tag{16}$$

Substituting the above results into eqn. (12), we obtain the mobility of a Li^+ vacancy at the position A:

$$\mu_A = \frac{|e|\nu\beta a^2}{2} exp(-\beta G_{Li}^m). \tag{17}$$

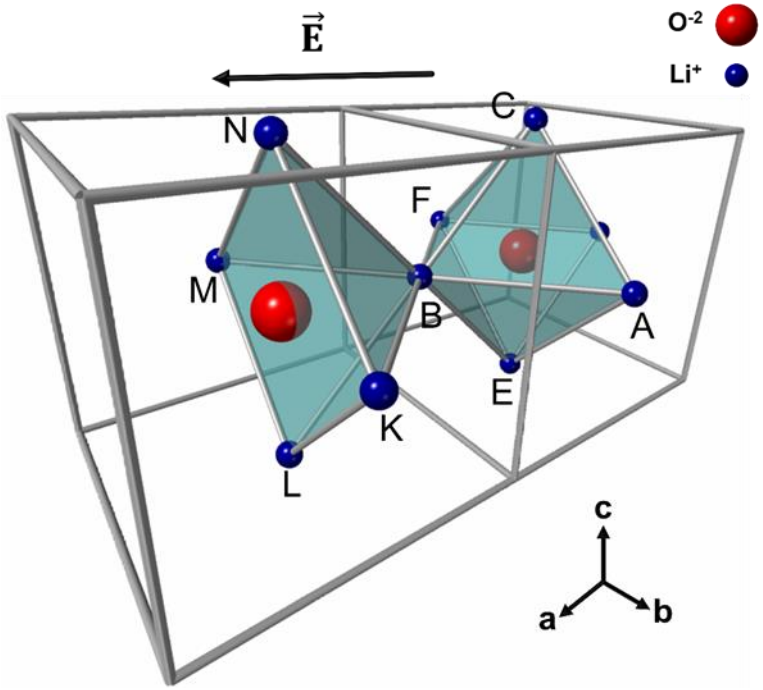

Fig. S5. Scheme utilized to calculate the mobility of a Li^+ ion vacancy (not shown) at position B, based on the eight neighbouring positions to which such vacancy can hop, namely A, C, E, F, K, L, M, and N.

Next, we consider the mobility of a Li^+ ion vacancy at position B. Such vacancy can move to any of the eight nearby Li^+ ion positions shown in Fig. S5. Since any of these displacements correspond to a migration distance of half lattice parameter along the electric field direction, we have

$$|\rho_{B\to Y}|^2 = \frac{a^2}{4}; Y = A, C, E, F, K, L, M, N. \tag{18}$$

Summing over all eight positions, we get

$$\sum_{j=Y} |\rho_{B\to Y}|^2 = 8\left(\frac{a^2}{4}\right) = 2a^2 \tag{19}$$

Substituting the above result into eqn. (12), we obtain the following expression for the of a Li^+ vacancy at the position B:

$$\mu_B = |e|\nu\beta a^2 exp(-\beta G_{Li}^m) \tag{20}$$

For a Li^+ ion vacancy at position C, we have the scheme shown in Fig. S6. We have contributions of half lattice parameter for projected distances from C to B, D, P and R positions,

$$|\rho_{C\to Y}|^2 = \frac{a^2}{4}; \quad Y = B, D, P, R, \tag{21}$$

and zero otherwise,

$$|\rho_{C\to Y}|^2 = 0; \quad Y = A, F, O, Q. \tag{22}$$

Therefore, the mobility of a Li^+ vacancy at the position C is given by:

$$\mu_C = \frac{|e|\nu\beta a^2}{2} exp(-\beta G_{Li}^m). \tag{23}$$

Now we can finally calculate the mean mobility of Li^+ vacancies:

$$\langle \mu_{Li} \rangle = \frac{\mu_A + \mu_B + \mu_C}{3}; \tag{24}$$

$$\boxed{\langle \mu_{Li} \rangle = \frac{2|e|\nu\beta a^2}{3} exp(-\beta G_{Li}^m)}. \quad (25)$$

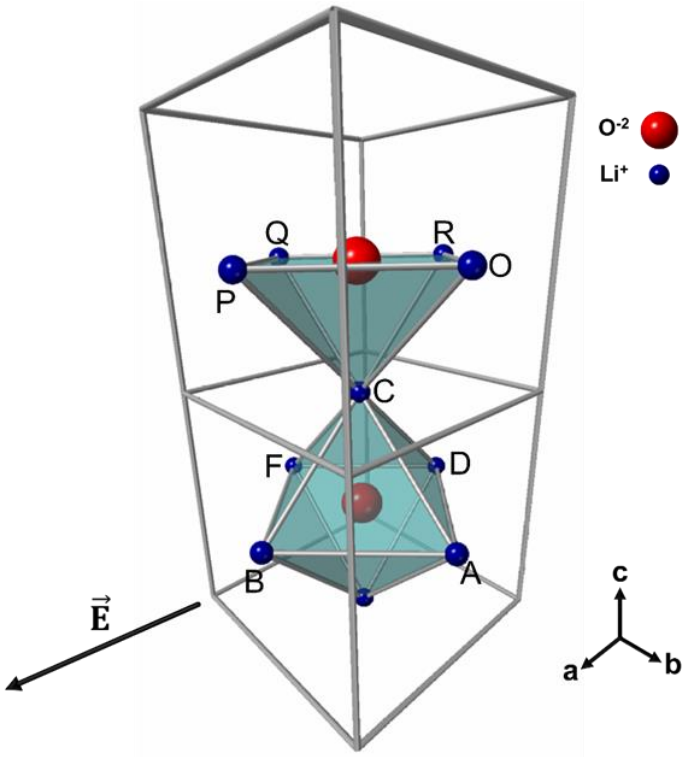

Fig. S6. Scheme utilized to calculate the mobility of a Li^+ ion vacancy (not shown) at position C, based on the eight nearby positions to which such vacancy can hop, namely A, B, D, F, O, P, Q, and R.

3.2 Electrical mobility of Cl^- vacancies

There is only one possible position that a Cl^- vacancy can occupy in a unit cell (position A, in Fig. S7), so no average is needed to calculate its electrical mobility, μ_{Cl}. Although there are seven other positions in the unit cell's corners, they belong to the neighbouring cells. Therefore, to obtain μ_{Cl}, suffices to calculate the Cl^- vacancy mobility at the position A.

As we did for Li^+ vacancies, the starting point is eqn. (12). Here also, all the Gibbs energies of migration are the same, and the electric field is oriented in the same direction, and orientation, as the lattice parameter $\vec{a}$. Thus,

$$\mu_A = \frac{|e|\nu\beta}{2} exp(-\beta G_{Cl}^m) \sum_{\gamma} \left(\rho_{A\to\gamma}\right)^2, \quad (26)$$

where G_{Cl}^m is the Gibbs energy of migration of a Cl^- vacancy *via* Path L1 (as discussed in the main text). The only two migrations that lead to a nonzero displacement distance in the electric field's direction are from A to either B or D, both a lattice parameter-long. Therefore, the electrical mobility of a Cl^- vacancy is

$$\mu_A = |e|\nu\beta a^2 exp(-\beta G_{Cl}^m); \quad (27)$$

$$\boxed{\mu_{Cl} = |e|\nu\beta a^2 exp(-\beta G_{Cl}^m)}. \quad (28)$$

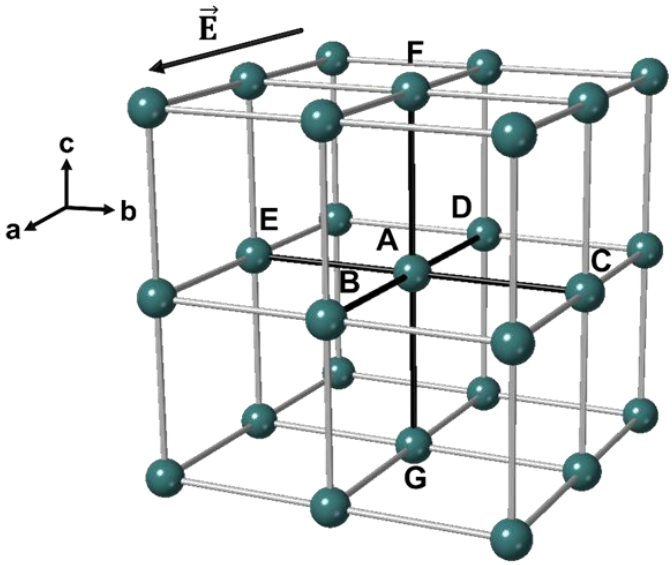

Fig. S7. Scheme utilized to calculate the mobility of a Cl^- ion vacancy (not shown) at position A, based on the six nearby positions to which such vacancy can hop, namely B, C, D, E, F and G.

4 Probability of a jump via Path S1 before the jump via Path S2 reverses

After the first migration, the probability that neither the second migration nor the reversal of the first one happens for $n-1$ attempts, with the second migration happening in the nth attempt, is

$$p(n) = (1-p_r)^{n-1}(1-p_2)^{n-1}(1-p_r)p_2 = (1-p_r)^n(1-p_2)^{n-1}p_2, \tag{29}$$

where for each attempt,

$$p_r = \exp\left(-\beta G_{S2r}^m\right) \tag{30}$$

is the probability of reversal and

$$p_2 = \exp\left(-\beta G_{S1}^m\right), \tag{31}$$

is the probability of the second migration happening. Here, G_{S2r}^m is the Gibbs energy of migration via Path S2, but in the reverse direction.

The number of attempts made in t seconds is $N = t\nu$, where ν is the attempt frequency (taken as 10 THz here). Thus, the probability of the second migration happening in N or fewer attempts without reversal is

$$\begin{aligned} p(n \le t\nu) &= \frac{p_2}{1-p_2}\sum_{n=1}^{t\nu}[(1-p_r)(1-p_2)]^n \\ &\approx \frac{p_2(1-p_r)}{1-(1-p_r)(1-p_2)}. \end{aligned} \tag{32}$$

The latter approximation takes into account that for t of the order of seconds, $t\nu \to \infty$, and we obtain an infinite sum of a geometric series. It is worth noting that this result does not depend on t. This reflects the fact that the larger n is, the smaller $p(n)$ is, in a way that the series has already reached convergence for times of the order of seconds.

Assuming the Gibbs energy of migration of a Cl^- ion via Path S1 does not change much due to the O_{Cl}' antisite (formed after the O^{2-} migration via Path S2), we can estimate $p(n \le t\nu)$ at 550 K from $G_{S1}^m(550\ K) = 0.628$ eV and $G_{S2r}^m(550\ K) = 0.068$ eV as approximately 6×10^{-6}.

5 On the calculation of concentration profiles

We assume a spherical grain (of diameter $2R$), in accord with experimental evidence.[11] Also, since Li_3OCl has cubic symmetry, diffusion is isotropic (in the absence of external fields). Thus, the diffusivity D is scalar and the diffusion equation writes:

$$\frac{1}{D}\frac{\partial c(r,t)}{\partial t} = \nabla^2 c(r,t) = \frac{\partial^2 c(r,t)}{\partial r^2} + \frac{2}{r}\frac{\partial c(r,t)}{\partial r}, \tag{33}$$

where $c(r,t)$ is the concentration of vacancies (number of vacancies per unit of volume) at a distance r from the centre of the grain at time t.

Due to the grain's spherical symmetry, we assume that the concentration has the form

$$c(r,t) = \gamma + T(t)R(r), \tag{34}$$

where γ is a constant; $T(t)$ and $R(r)$ are functions of time and position, respectively. This assumption allows us to separate the diffusion equation in

$$\frac{1}{D}\frac{1}{T(t)}\frac{\partial T(t)}{\partial t} = -k^2 \tag{35}$$

and

$$\frac{1}{R(r)}\frac{\partial^2 R(r)}{\partial r^2} + \frac{2}{rR(r)}\frac{\partial R(r)}{\partial r} = -k^2\,, \tag{36}$$

with general solutions

$$T(t) = T(0)e^{-k^2 Dt} \tag{37}$$

and

$$R(r) = A\frac{sin(kr)}{r} + B\frac{cos\,(kr)}{r}\,. \tag{38}$$

By taking a linear combination of the possible solutions and enforcing that the overall solution must be finite at $r = 0$, we get:

$$c(r,t) = \gamma + \sum_{n=1}^{\infty} F_n \frac{sin(k_n r)}{r} e^{-k_n^2 Dt} \tag{39}$$

We determined the coefficients F_n, k_n, and γ by the boundary and initial conditions of the problem:

- Final:

$$c(r,\infty) = c_{surf} \tag{40}$$

- Initial:

$$c(r,0) = \begin{cases} c_{surf}, & r = R \\ c_0, & 0 \le r < R \end{cases} \tag{41}$$

- Boundary:

$$\begin{cases} c(R,t) = c_{surf} \\ \left.\dfrac{\mathrm{d}c(r,t)}{\mathrm{d}r}\right|_{r=0} = 0 \end{cases} \tag{42}$$

In the equations above, c_0 and c_{surf} are the initial concentration in the grain interior and the surface concentration, respectively. Such conditions lead to the following solution:

$$c(r,t) = c_{surf} + \frac{2(c_0 - c_{surf})R}{r\pi}\sum_{n=1}^{\infty}\frac{(-1)^{n+1}}{n} sin\left(\frac{n\pi r}{R}\right) e^{-n^2\pi^2 Dt/R^2}\,. \tag{43}$$

By making explicit the temperature dependence through D, we have:

$$c(r,t,T) = c_{surf} + \frac{2(c_0 - c_{surf})R}{r\pi}\sum_{n=1}^{\infty}\frac{(-1)^{n+1}}{n} sin\left(\frac{n\pi r}{R}\right) e^{-n^2\pi^2 D(T)t/R^2}\,. \tag{44}$$

We can convert c into η – number of vacancies per unit formula – using the expression

$$\eta = a^3 c \,, \tag{45}$$

since there is only one unit formula per unit cell. Here, a is the temperature-dependent lattice parameter of the cubic unit cell.

References

1 B. Dick and A. Overhauser, Theory of the dielectric constants of alkali halide crystals, *Phys. Rev.*, 1958, **112**, 90–103.

2 J. D. Gale and A. L. Rohl, The General Utility Lattice Program (GULP), *Mol. Simul.*, 2003, **29**, 291–341.

3 H. J. Monkhorst and J. D. Pack, Special points for Brillouin-zone integrations, *Phys. Rev. B*, 1976, **13**, 5188–5192.

4 N. L. Allan, T. H. K. Barron and J. A. O. Bruno, The zero static internal stress approximation in lattice dynamics, and the calculation of isotope effects on molar volumes, *J. Chem. Phys.*, 1996, **105**, 8300–8303.

5 M. B. Taylor, G. D. Barrera, N. L. Allan, T. H. K. Barron and W. C. Mackrodt, Shell: a code for lattice dynamics and structure optimisation of ionic crystals, *Comput. Phys. Commun.*, 1998, **109**, 135–143.

6 M. B. Taylor, G. D. Barrera, N. L. Allan and T. H. K. Barron, Free-energy derivatives and structure optimization within quasiharmonic lattice dynamics, *Phys. Rev. B*, 1997, **56**, 14380–14390.

7 R. Mouta, M. Á. B. Melo, E. M. Diniz and C. W. A. Paschoal, Concentration of Charge Carriers, Migration, and Stability in Li_3OCl Solid Electrolytes, *Chem. Mater.*, 2014, **26**, 7137–7144.

8 M. Kilo, Modeling of cation diffusion in oxygen ion conductors using molecular dynamics, *Solid State Ionics*, 2004, **175**, 823–827.

9 A. B. Lidiard, in *Handbuch der Physik*, Springer Berlin Heidelberg, Berlin, Heidelberg, 1957, pp. 246–349.

10 D. Lynch, Diffusion and Ionic Conductivity in Cesium Bromide and Cesium Iodide, *Phys. Rev.*, 1960, **118**, 468–473.

11 M. Dondelinger, J. Swanson, G. Nasymov, C. Jahnke, Q. Qiao, J. Wu, C. Widener, A. M. Numan-Al-Mobin and A. Smirnova, Electrochemical stability of lithium halide electrolyte with antiperovskite crystal structure, *Electrochim. Acta*, 2019, **306**, 498–505.